


Article

Potential of *Staphylea holocarpa* Wood for Renewable Bioenergy

Yiyang Li ^{1,†} , Erdong Liu ^{2,†}, Haiping Gu ¹, Junwei Lou ^{3,*}, Yafeng Yang ¹, Longhai Ban ^{4,*}, Wanxi Peng ^{1,*} and Shengbo Ge ^{5,*} ¹ School of Forestry, Henan Agricultural University, Zhengzhou 450002, China² Department of Agricultural and Forestry Sciences, Henan Zhumadian Agricultural School, Zhumadian 463000, China³ School of Architectural Engineering, Zhejiang Business Technology Institute, Ningbo 315012, China⁴ Office of Academic Research, State Owned Madao Forest Farm of Biyang County, Zhumadian 463000, China⁵ Jiangsu Co-Innovation Center of Efficient Processing and Utilization of Forest Resources, College of Materials Science and Engineering, Nanjing Forestry University, Nanjing 210037, China

* Correspondence: 10815018@zjbt.net.cn (J.L.); banlh@126.com (L.B.); pengwanxi@163.com (W.P.); geshengbo@njfu.edu.cn (S.G.)

† These authors contributed equally to this work.

Abstract: Energy is indispensable in human life and social development, but this has led to an overconsumption of non-renewable energy. Sustainable energy is needed to maintain the global energy balance. Lignocellulose from agriculture or forestry is often discarded or directly incinerated. It is abundantly available to be discovered and studied as a biomass energy source. Therefore, this research uses *Staphylea holocarpa* wood as feedstock to evaluate its potential as energy source. We characterized *Staphylea holocarpa* wood by utilizing FT-IR, GC-MS, TGA, Py/GC-MS and NMR. The results showed that *Staphylea holocarpa* wood contained a large amount of oxygenated volatiles, indicating that it has the ability to act as biomass energy sources which can achieve green chemistry and sustainable development.

Keywords: *Staphylea holocarpa*; lignocellulose; GC-MS; Py/GC-MS; NMR

Citation: Li, Y.; Liu, E.; Gu, H.; Lou, J.; Yang, Y.; Ban, L.; Peng, W.; Ge, S. Potential of *Staphylea holocarpa* Wood for Renewable Bioenergy. *Molecules* **2023**, *28*, 299. <https://doi.org/10.3390/molecules28010299>

Academic Editors: Lukasz Klapiszewski and Teofil Jesionowski

Received: 30 November 2022

Revised: 24 December 2022

Accepted: 26 December 2022

Published: 30 December 2022



Copyright: © 2022 by the authors. Licensee MDPI, Basel, Switzerland. This article is an open access article distributed under the terms and conditions of the Creative Commons Attribution (CC BY) license (<https://creativecommons.org/licenses/by/4.0/>).

1. Introduction

Human civilization has reached a new historical height with current developments in science and technology, but it has also increased its utilization of energy simultaneously. Energy is extremely important for the development of the material basis and society, and is particularly important economically [1]. As an important material base, energy has played an indispensable role in nation building and human development. These include GDP growth, social and scientific development and the security of the nation [2]. At present, most countries in the world are still obtaining most of their energy from fossil energy [3]. However, the drastic reduction in fossil energy and the ecological environment has brought many problems. Therefore, it is necessary to develop renewable energy in order to alleviate the over-consumption of non-renewable energy [4].

Biomass is an important energy source in renewable energy because it can achieve carbon neutrality. Biomass has many advantages, such as diversity, practicality and sustainability [5]. Biomass can be turned into usable energy through a variety of methods, including physical and chemical methods. Examples of biomass include plants, forest waste, animal waste and municipal solid waste, etc. [6]. According to the World Bioenergy Association statistical report, biomass accounted for 9.5% of all energy supply and contributed about 55.6 EJ of energy in 2017. The greatest contribution to bioenergy belongs to the forestry sector, where forestry biomass has contributed up to 85% of the total energy [7,8].

Bioenergy is obtained mostly from wood biomass, and wood-based bioenergy development can play a vital role in achieving energy independence, reducing carbon emissions and promoting rural development [9]. With the advent of advanced afforestation treatments and efficient biotechnology, wood-based bioenergy development can meet the needs of sustainable energy production [10]. About 11% of the world's primary energy consumption comes from biomass. However, material shortage in wood-based biomass urgently needs an alternative source for bioenergy production. For example, *Eucalyptus pellita* and *Hevea brasiliensis* clones are potential woods for bioenergy production, with a net calorific value of 16,502 kJ kg⁻¹ and 19,757 kJ kg⁻¹, respectively [11]. *Tachigali vulgaris* planted at a land greater than 6 m² has a net calorific value more than 7.95 MJ/kg, and a medium basic density which is suitable for bioenergy production [12]. Buss et al. found that using native willow fragments for 2–37 years can yield greenhouse gas benefits within 0–20 years in Fort McPherson, Northwest Territories, Canada [13]. *Pinus* spp. and *Quercus* spp. were pressed into solid biofuel blocks that can be used to meet the need to generate low-power heat for the residential sector. The preparation of solid biofuel blocks from biomass residues is efficient, economical and easy to manufacture and use [14].

Lignocellulosic biomass is the most widespread biological resource on earth and can be transformed into value-added by-products, including biomass materials, bio-oils and biofuels [15,16]. Lignocellulosic biomass has been well recognized in the production of chemicals and wood biomaterials [17]. Lignocellulosic biomass can be found in almost all types of plants, and it does not affect food security or biodiversity or cause pollution to the environment [18,19]. Cellulose, hemicellulose and lignin make up lignocellulosic biomass; it is a complex polymer material. [20–22]. Lignocellulosic biomasses are rich in phenols, carbohydrates, lipids and pectin, which has the potential to be converted into valuable liquid or gaseous biofuels [23]. Lignocellulosic materials can also be converted into bioethanol or biomethanol after treatment [24,25]. The utilization of lignocellulosic biomass can help to improve the forestry economy and generate additional income for society, as well as create employment opportunities for people [26,27].

Staphylea holocarpa Hemsl. (*S. holocarpa*) is an endemic plant in China; it is a small deciduous tree belonging to staphyleaceae. *S. holocarpa* has compound leaves (three leaflets), and smooth and glabrous branchlets. Its flowers are pear-shaped bulging capsules, and usually pink in color. It blooms from April to May and ripens in September, which is of ornamental value [28]. *S. holocarpa* can be found throughout China, including in Henan, Anhui and Shanxi, generally on limestone slopes of deciduous forests at altitudes of about 900–1000 m [29]. The bark of *S. holocarpa* is rich in cellulose. The seeds are pressed and used in soap and paint production [30]. *S. holocarpa* root has the functions of moisturizing the lungs and relieving coughs, dispelling wind and dampness; this is of great developing value in the utilization of wild economic plants [31]. Tian studied the diverse distribution of *S. holocarpa* plants, including 13 distribution types and 10 variations. According to the distribution area types of the genus, *S. holocarpa* has obvious temperate characteristics. With the increase in altitude, the population structure changed from growing to stable [32].

To the best of author's knowledge, limited research has been reported about *S. holocarpa* wood, especially in the field of bioenergy. Therefore, this article begins with *S. holocarpa* wood as a subject of research on its latent as a lignocellulosic bioenergy source. The active component of *S. holocarpa* wood was extracted and was characterized with FT-IR, GC-MS and TGA. The Py/GC-MS and NMR were used to detect the pyrolysis product and characterize the composition, functional groups and thermal stability from pyrolysis of *S. holocarpa* wood.

2. Results and Discussion

2.1. FT-IR Analysis

In this experiment, the FT-IR of four *S. holocarpa* wood extracts were analyzed in the range of 4000–550 cm⁻¹ (Figure 1). Different functional groups were observed in the four extracts. All samples showed bands around 3376 cm⁻¹, indicating tensile vibrations of

intermolecular H–O–H [33,34]. The tensile vibrations of $-\text{CH}_2-$ in alkanes were mainly distributed in the range of 2976 – 2837 cm^{-1} [35]. Due to the presence of ester acids and aromatic components, there were C=C and C=O stretching at 1655 cm^{-1} [36]. Bands close to 1927 cm^{-1} also represent =O stretching, and the high wave number may occur due to the induced effect of C–F substituents. The absorption peaks at 1454 , 1414 , 1412 and 1380 cm^{-1} belong to C–H stretching [37]. There is a small absorption peak at 1275 cm^{-1} in *S. holocarpa* wood ethanol, ethanol/benzene and ethanol/methanol extracts, but not in *S. holocarpa* wood methanol extract, representing $-\text{CH}_3$ bonds [38]. Due to $-\text{O}$ vibration, there were overlapping peaks between 1090 and 1115 cm^{-1} [39]. In particular, the deep bands at 1026 cm^{-1} (A1 extract) and 1051 cm^{-1} (the other three extracts) indicate $-\text{O}$ stretching in the tetrahedral sheet [40]. The formation of peaks at 1090 and 1053 cm^{-1} was due to C–O–C and $-\text{OH}$ vibrations. Thus, $-\text{OH}$, together with the peak assigned to the aromatic ring (1655 cm^{-1}), indicates the presence of phenols [41].

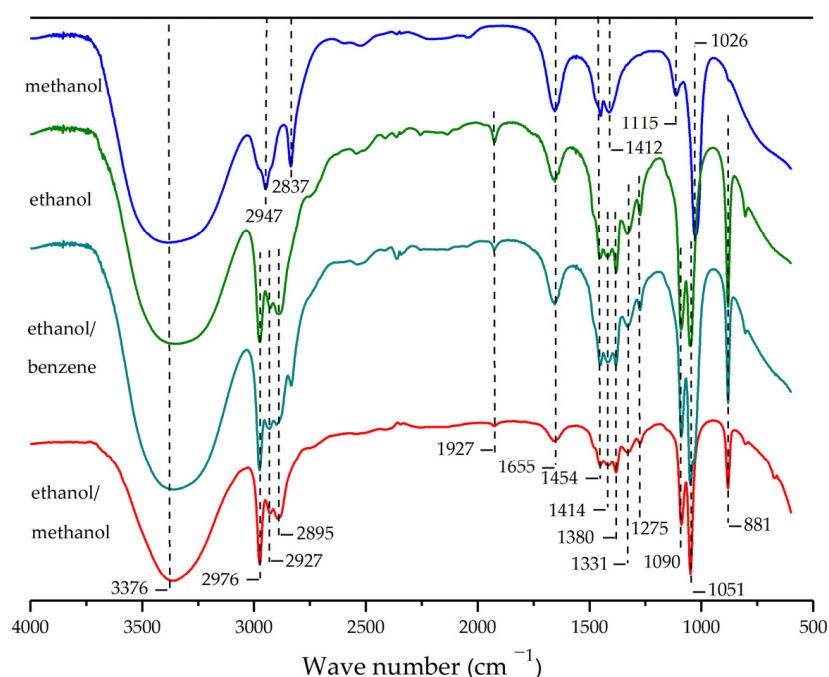


Figure 1. FT-IR spectra of four extract samples of *S. holocarpa* wood. Methanol, ethanol, ethanol/benzene, and ethanol/methanol extract samples are represented by the blue line, green line, blue-green line, and red line, respectively.

All spectra exhibit similar spectral signatures, except for differences in infrared absorption intensity. Typical aromatic bands of lignin were at 1655 and 1454 cm^{-1} (Figure 1) [42]. These samples were rich in carbon, because the transmission intensity of each peak gradually increases as the type of carbon changes. In contrast, the number of absorption peaks in *S. holocarpa* wood ethanol, ethanol/benzene and ethanol/methanol extracts were greater than in *S. holocarpa* wood methanol extract, and absorption peaks were associated with $-\text{CH}_3$ bonds [43]. The FT-IR spectrum showed no $-\text{C}\equiv\text{C}-$ vibrations at 2140 – 2100 cm^{-1} , indicating the absence of a $\text{C}\equiv\text{C}$ functional group in *S. holocarpa* wood (Figure 1). Another possible reason is that during the extraction process, some chemical bonds become unstable, or condense under high temperature conditions [44]. In general, the main chemical components of *S. holocarpa* wood samples characterized by FT-IR testing include phenols, alcohols, acids, and hydrocarbons. The absorption peaks of the four sample extracts were mainly distributed at 3800 – 3030 cm^{-1} , 3030 – 2835 cm^{-1} , and 1500 – 881 cm^{-1} .

2.2. GC–MS Analysis

GC–MS detection results show that 15, 37, 27 and 44 chemical components were identified from four extracts of *S. holocarpa* wood, which were ethanol, methanol, benzene/ethanol, and ethanol/methanol, respectively (Figure 2). More specifically, they were as follows: 2-furanmethanol (1.37%), dihydroxyacetone (8.88%), 5-hydroxymethylfurfural (20.26%), 1,2,3-propanetriol, 1-acetate (6.55%), D-galactose (2.84%) (Table S1). Furfural (4.99%), butyl 2-acetoxyacetate (5.47%), 4-nonanol (2.36%), sucrose (4.91%), dl- α -tocopherol (20.75%) (Table S2). 1-hexanol, 2-ethyl- (47.63%), butyl 2-acetoxyacetate (4.01%), dibutyl phthalate (4.72%), 4-((1E)-3-hydroxy-1-propenyl)-2-methoxyphenol (3.94%), 2-propenoic acid, 3-(4-hydroxy-3-methoxyphenyl)- (0.56%) (Table S3). 2-furanmethanol (1.48%), ethanone, 1-(2-hydroxy-5-methylphenyl)- (3.04%), n-hexadecanoic acid (2.23%), linoelaidic acid (3.86%), 1,4-bis(trimethylsilyl)benzene (4.68%) (Table S4).

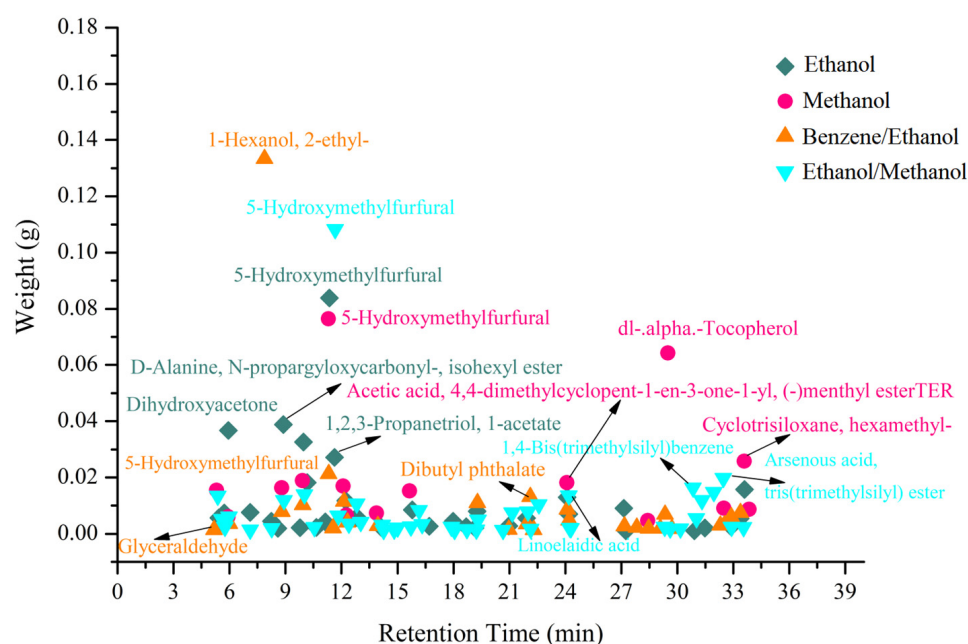


Figure 2. Total ion chromatograms of *S. holocarpa* wood four extract samples. Ethanol, methanol, benzene/ethanol, and ethanol/methanol extract samples are represented by the green square, purple circle, yellow triangle and blue triangle, respectively.

It can also be seen from Tables S1–S4 that the identified compounds can be divided into acids, alcohols, ketones, etc. *S. holocarpa* wood mainly contains 3-(4-hydroxy-3-methoxyphenyl)-2-acrylic acid, which has the potential to inhibit thrombosis, reduce inflammation, inhibit tumors and enhance sperm vitality. Clinically, 3-(4-hydroxy-3-methoxy-methoxy)-2-acrylic acid is mainly used for the vaso-assisted treatment of atherosclerosis, coronary heart disease, cerebrovascular disease, glomerular disease, pulmonary hypertension, etc., for phenyl. Furthermore, 3-(4-hydroxy-3-methoxy-methoxyacid)-2-acrylic acid can be used to treat migraines and vascular headaches, enhance hematopoietic function and treat leukocytopenia and thrombocytopenia [45–47]. dl- α -Tocopherol has many beneficial effects, such as eliminating pigment deposits in cells, slowing cell aging and promoting protein renewal synthesis, wound healing and the proliferation of capillaries and small blood vessels. In addition, it can improve the surrounding blood circulation and increase the oxygen supply in the tissues, thus creating good nutritional conditions for the healing of ulcers and antioxidants to protect cells from oxidative stress or damage [48,49].

In addition, many chemical components that are conducive to the development of biomass energy were detected in the four extracts. For example, furfural is an important biomass-derived platform molecule that can be used to synthesize a variety of value-added chemicals. Furfural and its derivatives are promising alternatives to traditional

petrochemicals [50]. The furfural industry is constantly evolving. Recently, the annual global production of furfural exceeded 300,000 tons, of which about 70% was produced in China [51]. Furfural and its derivatives are widely used in industrial production in organic solvents, pharmaceuticals, agricultural chemicals, biofuels and fuel additives [52]. One of the most important value-added products obtained from glycerin is dihydroxyacetone. Dihydroxyacetone can also be used as a building block in organic synthesis and is a promising area for the development of novel polymer biomaterials. One example is the design of injectable synthetic biodegradable polymer biomaterials composed of polyethylene glycol and a polycarbonate of dihydroxyacetone [53,54]. Among the various biomass-derived chemicals, 5-hydroxymethylfurfural has received great attention due to its potential applications, and is listed by the U.S. Department of energy as a promising platform chemical [55]. 5-hydroxymethylfurfural is a high-value central platform chemical that can be obtained directly from hexose dehydration. The unique structure of 5-hydroxymethylfurfural gives it high chemical activity and allows it to be transformed through various catalytic processes such as oxidation, hydrogenation and amination. It can be used in the production of high value-added chemicals and liquid fuels such as 2,5-furandialdehyde, 2,5-furandicarboxylic acid, levulinic acid, etc. [56]. In general, the chemical components identified via GC–MS from the *S. Holocarpa* wood extracts shows its potential in biomedicine and bioenergy. Thus, *S. Holocarpa* wood has the potential to be used as a lignocellulosic biomass source for bioenergy production.

2.3. TGA Analysis

The decomposition process of *S. holocarpa* wood was studied by TGA method in the range of 30–300 °C (rate of 20 °C/min). The changes in sample mass (TGA) and thermal degradation rate (DTG) are shown in Figure 3. According to the TGA curve, there were two distinct heat loss phases in *S. holocarpa* wood. The first stage occurs at temperatures around 83 °C and the weight of the wood was slightly reduced by 3.33%. As shown in the DTG curve, the maximum mass loss rate for this stage occurs at the first peak of 54 °C. There were reports that this stage was a drying process, where mass loss represents the removal of moisture and volatiles [57]. The weight reduction of *S. holocarpa* wood (3.33%) indicates that the wood has a certain moisture. The second phase of the mass reduction occurred in the range of 190–300 °C, and the wood mass was reduced by a total of 20.63% [58].

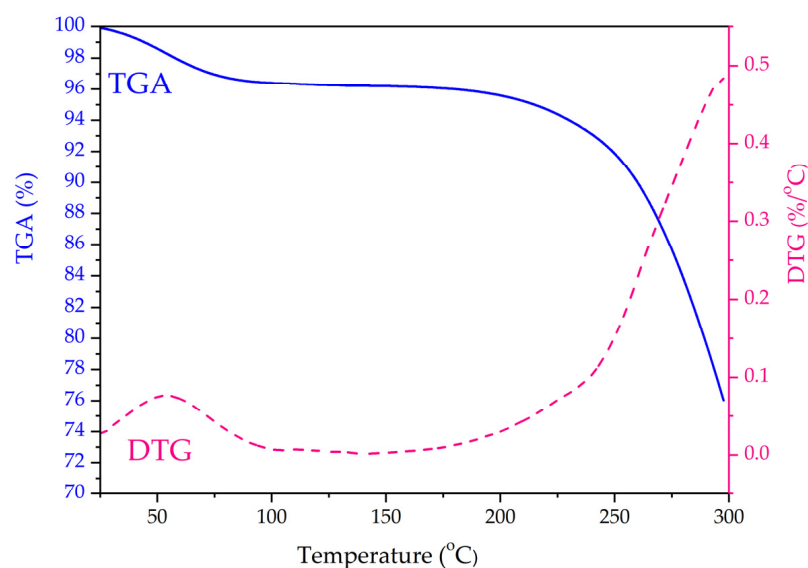


Figure 3. TGA–DTA curve of *S. holocarpa* wood.

The decomposition temperature of the wood biomass was about 190 °C; however, this decomposition temperature was delayed compared to some reported plants, such as *J. nudiflorum* wood biomass [59]. The DTG curve has a peak around 300 °C, indicating

that weight loss was fastest at this temperature. This stage was the active pyrolysis zone which belongs to the main stage of the volatile stage and pyrolysis mass loss [60]. The mass reduction was mainly due to the breakdown of lignocellulose's organic components. At this stage, the mass changes significantly, possibly caused by the changes in the chemical structure; chemical composition macromolecules were rapidly decomposed into more volatile small molecules at high temperatures [61]. The mass loss in the whole process of 0–300 °C is only 23.96%, and the heat loss is small, indicating that *S. holocarpa* wood has good thermal stability. In addition, the temperature set by this project was far from the carbonization temperature > 300 °C. Therefore, more volatile components can be obtained using this process [62].

2.4. Py/GC–MS Analysis

A total of 214 compounds were identified based on Py/GC–MS results (Figure 4). Among the compounds, the products of *S. holocarpa* wood pyrolysis at 500 °C were: ethyne, fluoro- (5.96%), dihydroxyacetone (4.22%), acetaldehyde (3.31%), ethyl ether (2.81%), hexadecanenitrile (2.33%), 2-propanone, 1-hydroxy- (2.11%), methyl glyoxal (2.07%), furfuryl alcohol, tetrahydro-5-methyl-, cis- (2.05%), etc. (see Table S5).

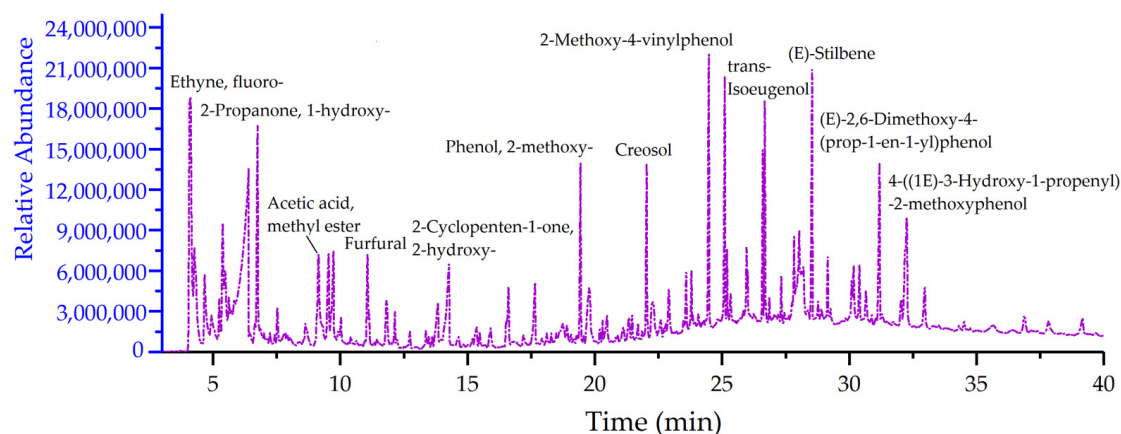


Figure 4. The total ion chromatography of *S. holocarpa* wood was determined by Py/GC–MS.

According to the statistics of Table S5, there are seven categories of ketones (48, 20.35%), aldehydes (13, 9.09%), acids (10, 3.09%), esters (18, 6.42%), alcohols (40, 15.64%), phenols (18, 18.69%), and ethers (5, 0.79%), of which the proportion of ketones (10.31%), alcohols (13.66%) and phenols (27.89%) were higher (Figure 5a). The pyrolysis of *S. holocarpa* wood is divided into three stages according to the time: <5 min, 5–25 min and >25 min; the pyrolysis products account for 10.795%, 47.546% and 41.695%, respectively (Figure 5b). In the <5 min stage, most of the pyrolysis products were small molecules of organic acids. In the 5–25 min stage, the pyrolysis products were mainly ketone compounds, and the reaction types were mainly double-bond reductions due to the presence of C=C and C=O. Most furan and cyclopentenones come from hemicellulose [63]. In the stage >25 min, the major component was phenolic substances and their derivatives produced by lignin pyrolysis. At the stage of 5–25 min, the pyrolysis products of the sample were the highest, indicating that the ketone content was high [64]. According to the properties of compounds at different stages, most of the compounds identified were organic acids, ketones, furans, cyclopentenones, phenols and their derivatives [65]. Most of these compounds are used in biopharmaceutical, chemical and energy industries [66,67].

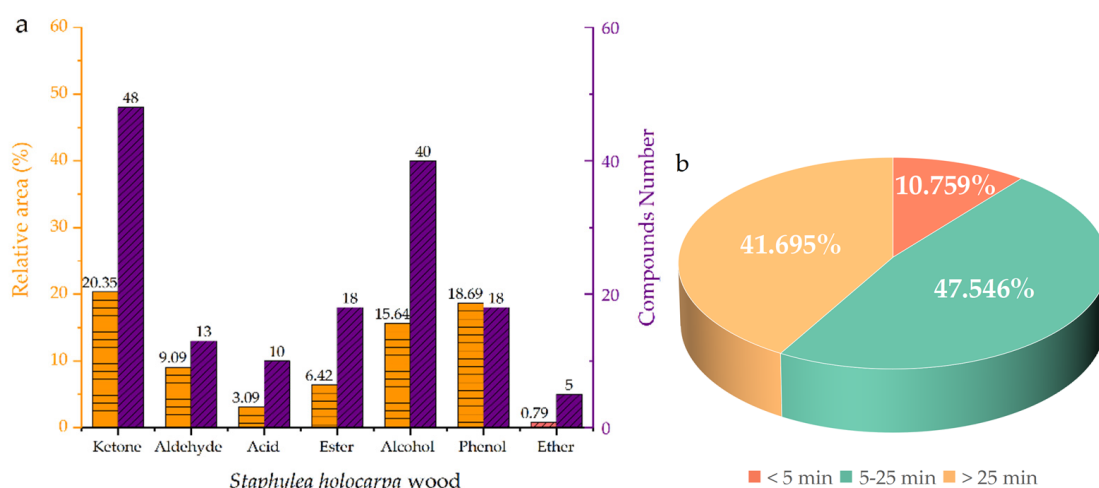


Figure 5. Classification (a) and temporal (b) distribution of pyrolysis products from *S. holocarpa* wood.

Many of the pyrolysis products identified by Py/GC–MS detection can be used in the chemical industry as green energy. For example, acetaldehyde belongs to biomass-derived oxygenated compounds, which are one of the main components of bio-oil. Acetaldehyde is mainly used as a reducing agent and is industrially used in the manufacturing of polyacetaldehyde, acetic acid, synthetic rubber, etc. [68]. Formic acid is a major product of carbohydrates derived from biomass and is receiving increasing attention as a sustainable hydrogen source. Formic acid-mediated biomass feedstock can be converted into value-added products, including biofuels, levulinic acid, etc. [69]. Catechol is an industrially relevant chemical with countless applications. It is the most representative basic structure unit in lignin, and it is also the main reaction intermediate and product in biomass or lignin pyrolysis [70]. Catechol plays an important role in many systems by interacting with organic and inorganic compounds. In addition, catechol crosslinked polymer networks exhibit remarkable mechanical strength, good adhesion and realistic properties [71].

Biomass provides an important source of raw materials, and is ideal for the development of functional or intermediate molecules for chemical synthesis, such as glycerol carbonate or glycidol [72]. Maltol is one of the derivatives of biomass, and maltol by-products have a certain synergistic effect with pine chips. Adding less than 10% maltol by-products to pine wood chips to make a fuel blend can improve combustion characteristics and reduce emissions [73]. 1,2-cyclopentanedione, 3-methyl- is an orthocyclodione, which is an important fine chemical intermediate and is widely used in pharmaceutical, chemical and other industries [74]. Phenol, 2-methyl- can be used in organic synthesis and also as a disinfectant and preservative; it is an important pharmaceutical intermediate. It is also the main compound in bio-oils [75]. Creosol is a lignin derivative of biomass and is a high value-added product, as a source of renewable assets of great interest to industry [76,77]. Similarly, the thermal cracking products detected by Py/GC–MS also contain chemical components such as furfural [50–52], dihydroxyacetone [53,54], and 5-hydroxymethylfurfural [55,56]. Analysis of pyrolysis products shows that the chemical components in *S. holocarpa* wood can be well applied in chemical, bioenergy and other fields. At the same time, the test results of Py/GC–MS and GC–MS were also consistent, which further demonstrates the potential of *S. holocarpa* wood for use as a source for bioenergy production.

2.5. NMR Analysis

2.5.1. ^1H -NMR Analysis

The ^1H -NMR spectrum of the nuclear magnetic resonance spectrum is the most widely used. It not only offers high magnetic detection sensitivity, but the signal is easy to observe; organic compounds provide a large number of hydrogen atoms in a variety of

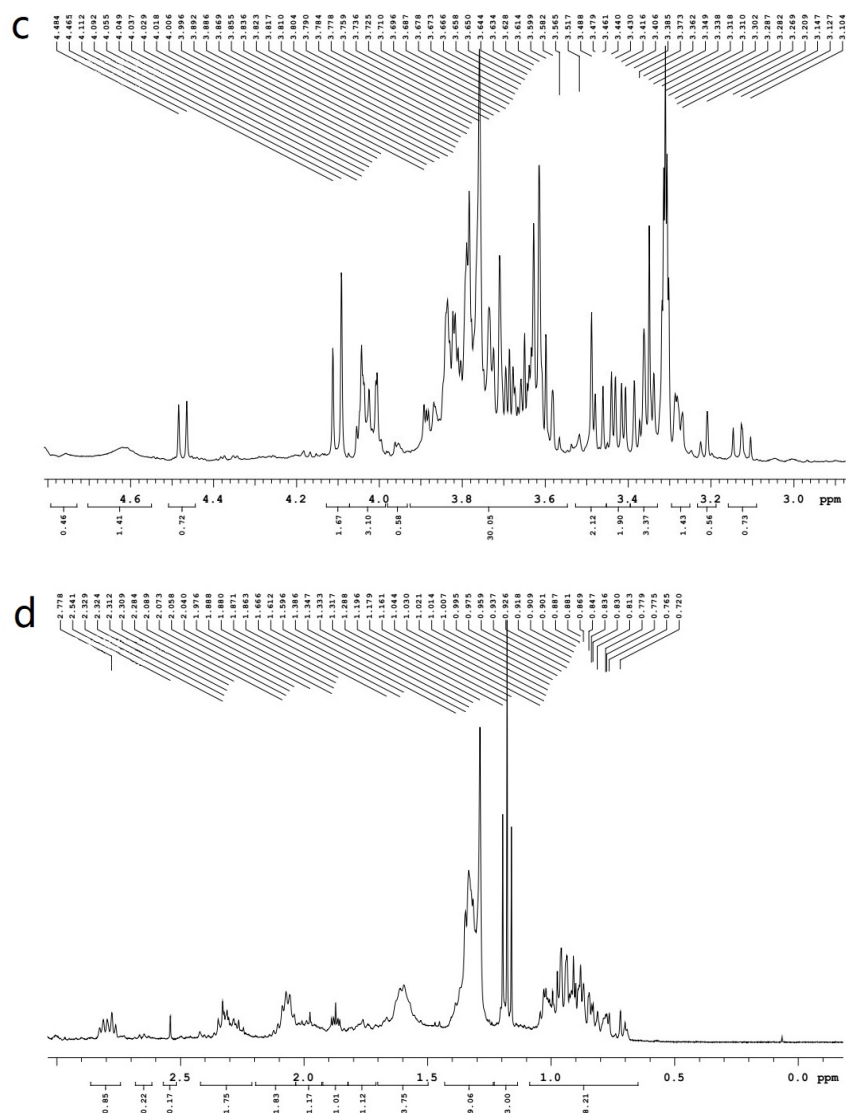


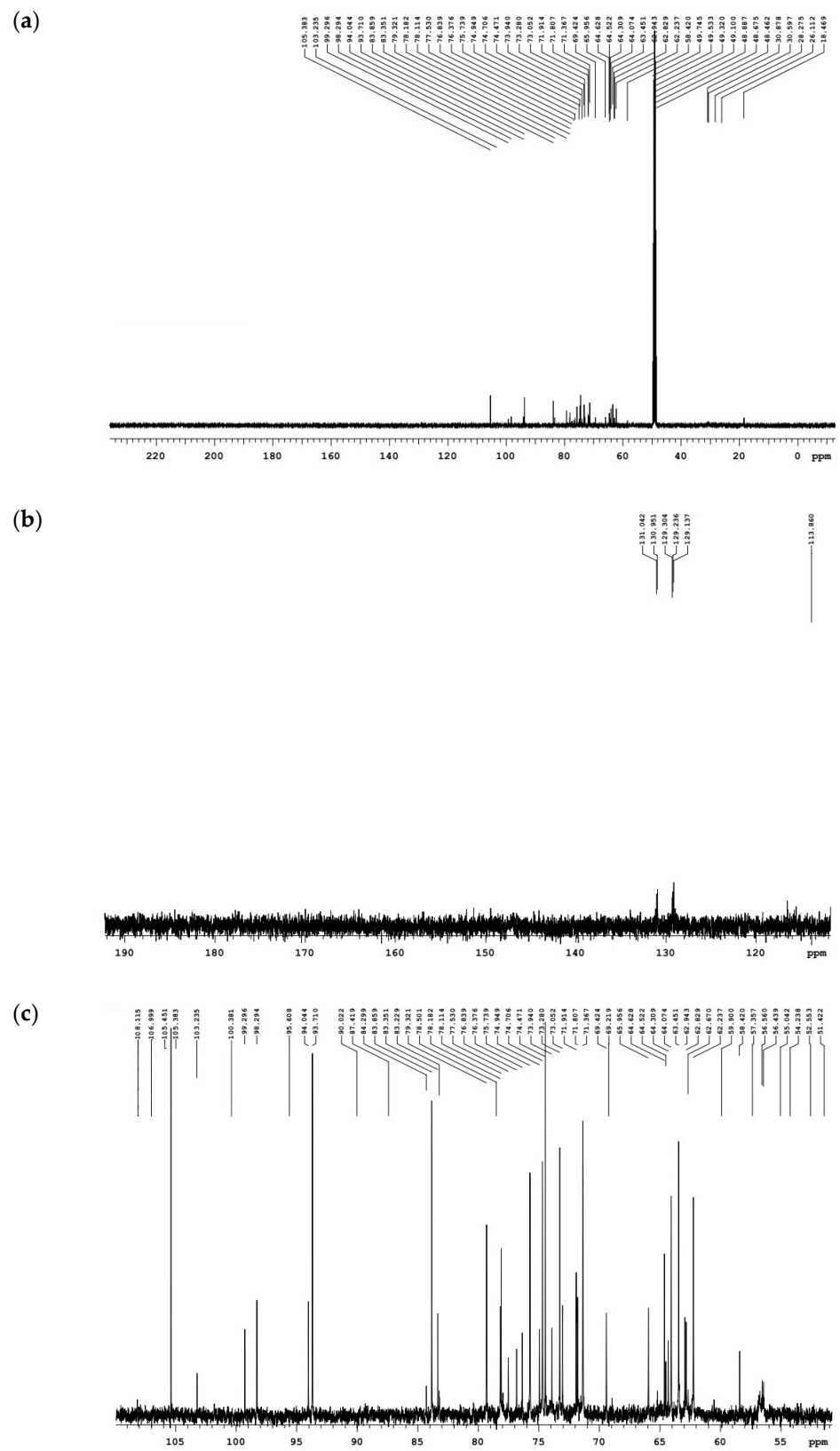
Figure 6. Total distribution of ^1H -NMR of *S. holocarpa* wood; (a–d) are enlarged views.

The results of ^1H -NMR detection showed that *S. holocarpa* wood was rich in chemical components, including acids, ethers, alcohols, esters, aromatics and other organic compounds. Bio-oil is a complex mixture of highly oxygenated organic components, including almost all types of oxygenated organic compounds. *S. holocarpa* wood has the potential to become a green and sustainable energy source. This was consistent with FT-IR, GC-MS, TGA and Py/GC-MS test results.

2.5.2. ^{13}C -NMR Analysis

Organic elements are the skeleton of carbon, currently ^{13}C -NMR spectroscopy is used to study the structure of sample changes through carbon atoms to understand the structure of organic compounds. Since some of the functional groups in the organic compound do not contain hydrogen atoms, these functional groups cannot be obtained from the ^1H spectrum and can only be obtained from the ^{13}C spectrum (Figure 7). For carbohydrates, the polymer carbon is mainly distributed in the 50–110 ppm region [81]. The carbon spectrum of saturated hydrocarbons, partial alkynes and partial olefins were mainly distributed between 15–45 ppm and 75–55 ppm. The carbon spectrum containing halogen elements (C-I: 0–40 ppm; c-bromine: 25–65 ppm; C-ci: 35–80 ppm) and the carbon spectrum of aromatic and olefins ($=\text{C}-$: 100–150 ppm; C_6H_6 : 110–160 ppm) were mainly distributed

between 0–80 ppm and 10–160 ppm. The signals at 20.3 ppm and 172.9 ppm shifts were mainly assigned to hemicellulose acetyl [[82–84](#)].



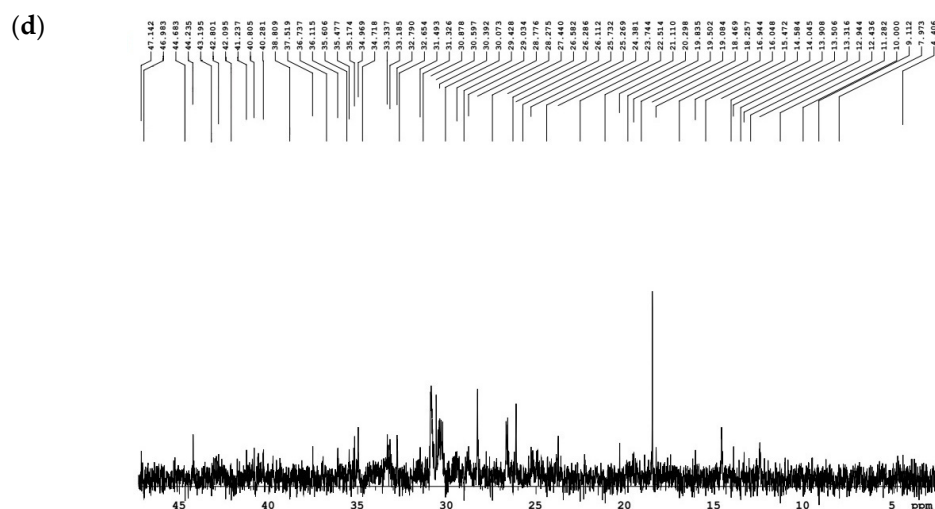


Figure 7. ^{13}C -NMR total distribution of *S. holocarpa* wood; (a–d) show enlarged views.

2.5.3. 2D-HSQC Analysis

In order to further understand the sample structure in more detail, 2D-HSQC NMR analysis was also carried out in this study. 2D-HSQC NMR is currently one of the most widely used technologies. Its ability to categorize functional groups clearly from 2D-HSQC maps provides an important structural shift in the sample and provides a resolution of overlapping signals in both ^1H and ^{13}C -NMR spectra, and analysis of two different aromatic groups [85]. In Figure 8, the aliphatic region of the HSQC spectrum was located at $\delta\text{C}/\delta\text{H}10\text{--}40/0.5\text{--}2.5$, the side chain was at $\delta\text{C}/\delta\text{H}50\text{--}95/2.5\text{--}6.0$ and the aromatic was at $\delta\text{C}/\delta\text{H}95\text{--}135/5.5\text{--}8.0$ [86]. $\delta\text{C}/\delta\text{H}92/5.3$, $\delta\text{C}/\delta\text{H}96/4.4$, $\delta\text{C}/\delta\text{H}102/6.6$, $\delta\text{C}/\delta\text{H}110/6.9$, $\delta\text{C}/\delta\text{H}115/6.7$, and $\delta\text{C}/\delta\text{H}120/6.8$. These chemical shifts indicate the interconnection between hydrogen atoms and carbon atoms [87]. As can be seen from the 2D-HSQC NMR chart, the linking of saturated hydrocarbons was at $\delta\text{C}/\delta\text{H}15\text{--}45/0.2\text{--}1.5$, the carbon spectra of partial alkynes and alkenes were $\delta\text{C}/\delta\text{H}55\text{--}75/1.7\text{--}3.5$, $4.5\text{--}5.9$, and the aromatic and olefinic carbons are located at $\delta\text{C}/\delta\text{H}110\text{--}140/6.3\text{--}8.5$, $4.5\text{--}5.9$, while the remaining alcohols, ethers, phenols and other oxygenates are located at $\delta\text{C}/\delta\text{H}60\text{--}80/3.3\text{--}4$ [88,89].

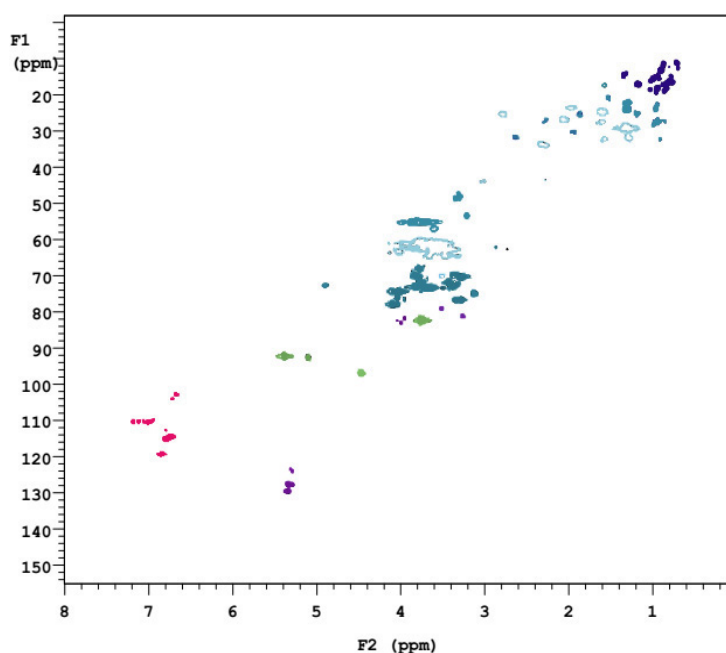


Figure 8. 2D-HSQC NMR spectra of the *S. holocarpa* wood sample.

3. Material and Methods

3.1. Sources of Sample and Extractives

S. holocarpa wood was collected from Xiaoqinling National Forest Park, Henan Province, and the wood sample was obtained from the trunk. The sample was processed into two different particle sizes, which were 40–60 μm and 200 μm powder. The powder with particle size of 40–60 μm was prepared for extraction, while the 200 μm powder was prepared for pyrolysis. About 15 g of the 40–60 μm powder was weighted, and extraction was performed in different organic solvents. Four types of organic solvent were prepared with optimum extraction temperature, including ethanol (75 $^{\circ}\text{C}$), methanol (65 $^{\circ}\text{C}$), benzene/ethanol (1:1) (90 $^{\circ}\text{C}$) and ethanol/methanol (1:1) (70 $^{\circ}\text{C}$). The extraction was performed for 5 h. After extraction, the four extracts were separated, and the excess solvent was removed with a rotary evaporator. The concentrated extracts were now ready for FT-IR and GC-MS analysis.

3.2. Experiment Methods

3.2.1. FT-IR Analysis

About 1 mL of extractives and 1 g KBr were mixed and pressed into KBr tablets which were, respectively, detected using a Thermo Fisher Nicolet iS10 FT-IR spectrophotometer (Waltham, MA, USA) by KBr method [90].

3.2.2. GC-MS Analysis

Each of the four extracts was tested on the Agilent-7890B-5977A (Santa Clara, CA, USA) instrument. Elastic quartz capillary columns (HP-5MS: 30 m \times 250 μm \times 0.25 μm) were used. The carrier gas flow rate was 1 mL/min; the carrier gas used was high purity helium, and the split ratio was set at 2:1. First, the temperature rises gradually from 50 $^{\circ}\text{C}$ to 250 $^{\circ}\text{C}$ at a rate of 8 $^{\circ}\text{C}/\text{min}$, and then from 250 $^{\circ}\text{C}$ to 300 $^{\circ}\text{C}$ at a rate of 5 $^{\circ}\text{C}/\text{min}$. The program was set to scan quality ranges, ionization voltages, ionization currents, ion sources and four-pole data for 30–600 amu, 70 eV, 150 ua, 230 $^{\circ}\text{C}$ and 150 $^{\circ}\text{C}$ [91].

3.2.3. TGA Analysis

Analysis of the 1 mg 200 μm powder was performed on a Perkin Elmer-STA8000 (Waltham, MA, USA) instrument. The temperature was set to rise from 30 $^{\circ}\text{C}$ –300 $^{\circ}\text{C}$ at the rate of 5 $^{\circ}\text{C}/\text{min}$. The carrier gas rate was set at 60 mL/min and the gas used was nitrogen [92].

3.2.4. Py/GC-MS Analysis

About 0.1 mg of the powder sample (200 μm) was placed in an Agilent-7890B-5977A CDS5000 (Santa Clara, CA, USA) instrument for analysis and detection. The carrier gas, pyrolysis temperature, heating rate and pyrolysis time used were helium (high purity), 500 $^{\circ}\text{C}$, 20 $^{\circ}\text{C}/\text{ms}$ and 15 s, respectively. The capillary column (HP-5MS: 60 m \times 250 μm \times 0.25 μm), pyrolysis product delivery line, injection valve temperature, shunt ratio and shunt velocity were 300 $^{\circ}\text{C}$, 300 $^{\circ}\text{C}$, 1:60 and 50 mL/min, respectively. The GC was programmed to last for 2 min at 40 $^{\circ}\text{C}$, increasing from 40 $^{\circ}\text{C}$ to 120 $^{\circ}\text{C}$ at a rate of 5 $^{\circ}\text{C}/\text{min}$. At 10 $^{\circ}\text{C}/\text{min}$, it went from 120 $^{\circ}\text{C}$ to 200 $^{\circ}\text{C}$ for 15 min. The MS ion source temperature and scanning range was 230 $^{\circ}\text{C}$ and 28–500 amu. [93].

3.2.5. NMR Analysis

The NMR polarizer model is Agilent-400 MR (Santa Clara, CA, USA) and methanol-d₄ was the solvent used in the testing process. The entire assay was performed with the same NMR probe: ¹H-NMR, ¹³C-NMR, and 2D-NMR. The duration, sample-and-hold time, pulse, pulse width and frequency of ¹H-NMR were 1.000 s, 2.556 s, 45 degrees, 6410.3 Hz and 399.79 MHz, respectively. The duration, sample-and-hold time, pulse, pulse width, frequency, hydrogen decoupling frequency and power of ¹³C-NMR are 1.000 s, 1.311 s, 45 degrees, 25,000 Hz, 100.53 MHz, 399.79 MHz and 38 dB, respectively. The duration, sample-and-hold time, pulse, pulse width, frequency, frequency of carbon decoupling and

power of 2D–HSQC are 1.000 s, 0.150 s, 4807.7 Hz, 20,105.6 Hz, 399.79 MHz, 100.54 MHz and 38 dB, respectively [94].

4. Conclusions

This project utilized *S. holocarpa* wood as the research object to evaluate its potential as a lignocellulosic biomass source for bioenergy production. The results proved that *S. holocarpa* wood contains a large amount of organic chemicals that can be used in the bioenergy and chemical industries. This project also provides the research basis of *S. holocarpa* wood pyrolysis, in which a large number of volatile compounds (including ketones, alcohols and phenol) were detected, which are proven to be important organic components of bio-oil. The NMR detection method used to identify the distribution of functional groups also proved that *S. holocarpa* wood has the potential to become a biomass energy source. This study explores the relationship between potential of the extraction and the pyrolysis of *S. holocarpa* wood, which is helpful for the exploitation and utilization of *S. holocarpa* wood as for bioenergy production. For the first time, NMR technology has been applied to *S. holocarpa* wood, and pyrolysis products show the potential to become high-value products. In the future, pyrolysis with various parameters can be optimized to maximize bioenergy production.

Supplementary Materials: The following supporting information can be downloaded at: <https://www.mdpi.com/article/10.3390/molecules28010299/s1>, Table S1: GC–MS analysis of ethanol sample; Table S2: GC–MS analysis of the methanol sample; Table S3: GC–MS analysis of benzene/ethanol sample; Table S4: GC–MS analysis of the ethanol/methanol sample; Table S5: Py/GC–MS analysis of *S. holocarpa* wood.

Author Contributions: Software, H.G.; Formal analysis, H.G.; Investigation, L.B.; Resources, E.L. and J.L.; Writing—original draft, Y.L. and E.L.; Writing—review & editing, Y.L. and Y.Y.; Supervision, J.L.; Project administration, S.G.; Funding acquisition, W.P. All authors have read and agreed to the published version of the manuscript.

Funding: The manuscript was supported by the Program for Central Plain Scholar Funding Project of Henan Province (No. 212101510005).

Institutional Review Board Statement: Not applicable.

Informed Consent Statement: Not applicable.

Data Availability Statement: The data presented in this study are available on request from the corresponding author.

Conflicts of Interest: The authors declare no conflict of interest.

References

1. Miao, C.; Fang, D.; Sun, L.; Luo, Q. Natural resources utilization efficiency under the influence of green technological innovation. *Resour. Conserv. Recycl.* **2017**, *126*, 153–161. [CrossRef]
2. Lee, C.C.; Xing, W. The impact of energy security on income inequality: The key role of economic development. *Energy* **2022**, *248*, 123564. [CrossRef]
3. Saidi, M.; Safaripour, M. Pure hydrogen and propylene coproduction in catalytic membrane reactor-assisted propane dehydrogenation. *Chem. Eng. Technol.* **2020**, *43*, 1402–1415. [CrossRef]
4. Skytt, T.; Nielsen, S.N.; Fröling, M. Energy flows and efficiencies as indicators of regional sustainability—A case study of Jämtland. *Sweden. Ecol. Indicat.* **2019**, *100*, 74–98. [CrossRef]
5. Fatma, S.; Hameed, A.; Noman, M.; Ahmed, T.; Shahid, M.; Tariq, M.; Sohail, I.; Tabassum, R. Lignocellulosic biomass: A sustainable bioenergy source for the future. *Protein Pept. Lett.* **2018**, *25*, 148–163. [CrossRef]
6. Nikolaidis, P.; Poullikkas, A. A comparative overview of hydrogen production processes. *Renew. Sustain Energy Rev.* **2017**, *67*, 597–611. [CrossRef]
7. World Bioenergy Association (WBA). Global Bioenergy Statistics. 2019. Available online: <https://www.worldbioenergy.org> (accessed on 10 November 2022).
8. Vries, W.; de Jong, A.; Kros, J.; Spijker, J. The use of soil nutrient balances in deriving forest biomass harvesting guidelines specific to region, tree species and soil type in The Netherlands. *For Ecol. Manag.* **2021**, *479*, 118591. [CrossRef]

9. Szulecka, J. Towards Sustainable Wood-Based Energy: Evaluation and Strategies for Mainstreaming Sustainability in the Sector. *Sustainability* **2019**, *11*, 493. [[CrossRef](#)]
10. Masum, M.F.H.; Sahoo, K.; Dwivedi, P. Ascertaining the Trajectory of Wood-Based Bioenergy Development in the United States Based on Current Economic, Social, and Environmental Constructs. *Annu. Rev. Resour. Econ.* **2019**, *11*, 169–193. [[CrossRef](#)]
11. Menucelli, J.R.; Amorim, E.P.; Freitas, M.L.M.; Zanata, M.; Cambuim, J.; de Moraes, M.L.T.; Yamaji, F.M.; da Silva, F.G.; Longui, E.L. Potential of Hevea brasiliensis Clones, Eucalyptus pellita and Eucalyptus tereticornis Wood as Raw Materials for Bioenergy Based on Higher Heating Value. *BioEnergy Res.* **2019**, *12*, 992–999. [[CrossRef](#)]
12. Silva, M.O.D.; da Silva, M.G.; Bufalino, L.; de Assis, M.R.; Goncalves, D.D.; Trugilho, P.F.; Protasio, T.D. Variations in productivity and wood properties of Amazonian tachi-branco trees planted at different spacings for bioenergy purposes. *J. Forestry Res.* **2021**, *32*, 211–224. [[CrossRef](#)]
13. Buss, J.; Mansuy, N.; Laganiere, J.; Persson, D. Greenhouse gas mitigation potential of replacing diesel fuel with wood-based bioenergy in an arctic Indigenous community: A pilot study in Fort McPherson, Canada. *Biomass Bioenerg.* **2022**, *159*, 106367. [[CrossRef](#)]
14. Morales-Maximo, M.; Ruiz-Garcia, V.M.; Lopez-Sosa, L.B.; Rutiaga-Quinones, J.G. Exploitation of Wood Waste of *Pinus* spp. for Briquette Production: A Case Study in the Community of San Francisco Pichataro, Michoacan, Mexico. *Appl. Sci.* **2020**, *10*, 2933. [[CrossRef](#)]
15. Bian, H.; Chen, L.; Dong, M.; Fu, Y.; Wang, R.; Zhou, X.; Wang, X.; Xu, J.; Dai, H. Cleaner production of lignocellulosic nanofibrils: Potential of mixed enzymatic treatment. *J. Clean. Prod.* **2020**, *270*, 122506. [[CrossRef](#)]
16. Parakh, P.D.; Nanda, S.; Kozinski, J.A. Eco-friendly transformation of waste biomass to biofuels. *Curr. Biochem. Eng.* **2020**, *6*, 120–134. [[CrossRef](#)]
17. Wang, S.; Dai, G.; Yang, H.; Luo, Z. Lignocellulosic biomass pyrolysis mechanism: A state-of-the-art review. *Prog. Energy Combust. Sci.* **2017**, *62*, 33–86. [[CrossRef](#)]
18. Valdivia, M.; Galan, J.L.; Laffarga, J.; Ramos, J.L. Biofuels 2020: Biorefineries based on lignocellulosic materials. *Microb. Biotechnol.* **2016**, *9*, 585–594. [[CrossRef](#)]
19. Chen, D.; Gao, A.; Cen, K.; Zhang, J.; Cao, X.; Ma, Z. Investigation of biomass torrefaction based on three major components: Hemicellulose, cellulose, and lignin. *Energy Convers. Manag.* **2018**, *169*, 228–237. [[CrossRef](#)]
20. Ge, S.B.; Manigandan, S.; Mathimani, T.; Basha, S.; Xia, C.L.; Brindhadevi, K.; Unpaprom, Y.; Whangchai, K.; Pugazhendhi, A. An assessment of agricultural waste cellulosic biofuel for improved combustion and emission characteristics. *Sci. Total Environ.* **2022**, *813*, 152418. [[CrossRef](#)]
21. Yang, J.L.; Ching, Y.C.; Chuah, C.H. Applications of Lignocellulosic Fibers and Lignin in Bioplastics: A Review. *Polymers* **2019**, *11*, 751. [[CrossRef](#)]
22. Ahmad, R.K.; Sulaiman, S.A.; Yusup, S.; Dol, S.S.; Inayat, M.; Umar, H.A. Exploring the potential of coconut shell biomass for charcoal production. *Ain Shams Eng. J.* **2022**, *13*, 101499. [[CrossRef](#)]
23. Alayoubi, R.; Mehmood, N.; Husson, E.; Kouzayha, A.; Tabcheh, M.; Chaveriat, L.; Sarazin, C.; Gosselin, I. Low temperature ionic liquid pretreatment of lignocellulosic biomass to enhance bioethanol yield. *Renew. Energy* **2020**, *145*, 1808–1816. [[CrossRef](#)]
24. Singh, N.; Singhania, R.R.; Nigam, P.S.; Dong, C.D.; Patel, A.K.; Puri, M. Global status of lignocellulosic biorefinery: Challenges and perspectives. *Bioresour. Technol.* **2022**, *344*, 126415. [[CrossRef](#)]
25. Albatrni, H.; Qiblaway, H.; Al-Marri, M.J. Walnut shell based adsorbents: A review study on preparation, mechanism, and application. *J. Water Process Eng.* **2022**, *45*, 102527. [[CrossRef](#)]
26. Awasthi, S.K.; Kumar, M.; Sarsaiya, S.; Ahluwalia, V.; Chen, H.; Kaur, G.; Sirohi, R.; Sindhu, R.; Binod, P.; Pandey, A.; et al. Multi-criteria research lines on livestock manure biorefinery development towards a circular economy: From the perspective of a life cycle assessment and business models strategies. *J. Clean. Prod.* **2022**, *341*, 130862. [[CrossRef](#)]
27. Ge, S.B.; Liang, Y.Y.; Zhou, C.X.; Sheng, Y.Q.; Zhang, M.L.; Cai, L.P.; Zhou, Y.H.; Huang, Z.H.; Manzo, M.; Wu, C.Y.; et al. The potential of *Pinus armandii* Franch for high-grade resource utilization. *Biomass Bioenerg.* **2022**, *158*, 106345. [[CrossRef](#)]
28. Yu, D.; Li, C.; Xie, K.; Zhang, G.; Gu, H.; Li, S. In Vitro Germination and Planlet Regeneration from Seeds of *Staphylea holocarpa*. *Subtrop. Plant Sci.* **2011**, *40*, 36–40.
29. Xu, B.; Shi, X.; Sun, Y.; Li, N. Study on Dormancy and Germination of *Staphylea Holocarpa* Hems1. *Seed* **2002**, *1*, 13–14.
30. Novotny, L.; Abdel-Hamid, M.E.; Hamza, H.; Masterova, I.; Grancai, D. Development of LC-MS method for determination of ursolic acid: Application to the analysis of ursolic acid in *Staphylea holocarpa* Hems1. *J. Pharmaceut. Biomed.* **2003**, *31*, 961–968. [[CrossRef](#)]
31. Lacikova, L.; Pferschy-Wenzig, E.M.; Masterova, I.; Grancai, D.; Bauer, R. Anti-inflammatory Potential and Fatty Acid Content of Lipophilic Leaf Extracts of Four *Staphylea* L. Species. *Nat. Prod. Commun.* **2009**, *4*, 543–546.
32. Tian, H.X. *Population Dynamics and Community Characteristics of Staphylea holocarpa in Yunqiu Mountain of Shanxi Province*; Shanxi Normal University: Xi'an, China, 2016.
33. Savchenko, D.; Vorlièek, V.; Kalabukhova, E.; Sitnikov, A.; Vasin, A.; Kysil, D. Infrared, Raman and Magnetic resonance spectroscopic study of SiO₂:C nanopowders. *J. Nano. Res. Lett.* **2017**, *12*, 292. [[CrossRef](#)] [[PubMed](#)]
34. Ge, S.B.; Brindhadevi, K.; Xia, C.L.; Elesawy, B.H.; Elfakhany, A.; Unpaprom, Y.; Van Doan, H. Egg shell catalyst and chicken waste biodiesel blends for improved performance, combustion and emission characteristics. *Fuel* **2021**, *306*, 121633. [[CrossRef](#)]

35. Shannon, M.; Lafeuille, J.L.; Fregiere-Salmomon, A.; Lefevre, S.; Galvin-King, P.; Haughey, S.A.; Burns, D.T.; Shen, X.Q.; Kapil, A.; McGrath, T.F.; et al. The detection and determination of adulterants in turmeric using fourier-transform infrared (FTIR) spectroscopy coupled to chemometric analysis and micro-FTIR imaging. *Food Control* **2022**, *139*, 109093. [[CrossRef](#)]
36. Cruz, M.D.; Van Schoors, L.; Benzarti, K.; Colin, X. Thermo-oxidative degradation of additive free polyethylene. part I. Analysis of chemical modifications at molecular and macromolecular scales. *J. App. Polym. Sci.* **2016**, *133*, 43287. [[CrossRef](#)]
37. Pandey, K.K. A study of chemical structure of soft and hardwood and wood polymers by FTIR spectroscopy. *J. App. Polym. Sci.* **2015**, *71*, 1969–1975. [[CrossRef](#)]
38. Liu, L.; Cheng, X.; Teng, L.; Wang, Y.; Dong, X.; Chen, L.; Zhang, D.; Peng, W.X. Systematic characterization of volatile organic components and pyrolyzates from *Camellia oleifera* seed cake for developing high value-added products. *Arab. J. Chem.* **2018**, *11*, 802–814. [[CrossRef](#)]
39. Kaya, E.M.Ö.; Özcan, A.S.; Özer, G.; Özcan, A. Adsorption kinetics and isotherm parameters of naphthalene onto natural- and chemically modified bentonite from aqueous solutions. *Adsorption* **2013**, *19*, 879–888. [[CrossRef](#)]
40. Soni, A.; Yusuf, M.; Mishra, V.K.; Beg, M. An assessment of thermal impact on chemical characteristics of edible oils by using FTIR spectroscopy. *Mater. Today* **2022**, *68*, 710–716. [[CrossRef](#)]
41. Gu, H.P.; Luo, X.Y.; Wang, H.Z.; Wu, L.S.; Wu, J.J.; Xu, J.M. The characteristics of phenanthrene biosorption by chemically modified biomass of *Phanerochaete chrysosporium*. *Environ. Sci. Pollut. Res.* **2015**, *22*, 11850–11861. [[CrossRef](#)]
42. Peng, W.X.; Maleki, A.; Rosen, M.A.; Pouria, A. Optimization of a hybrid system for solar-wind-based water desalination by reverse osmosis: Comparison of approaches. *Desalination* **2018**, *442*, 16–31. [[CrossRef](#)]
43. Alekhina, M.; Ershova, O.; Ebert, A.; Heikkinen, S.; Sixta, H. Softwood kraft lignin for value-added applications: Fractionation and structural characterization. *Ind. Crop. Prod.* **2015**, *66*, 220–228. [[CrossRef](#)]
44. Tomak, E.D.; Topaloglu, E.; Gumuskaya, E.; Yildiz, U.C.; Ay, N. An FT-IR study of the changes in chemical composition of bamboo degraded by brown-rot fungi. *Int. Biodeter. Biodegr.* **2013**, *85*, 131–138. [[CrossRef](#)]
45. Mancuso, C.; Santangelo, R. Ferulic acid: Pharmacological and toxicological aspects. *Food Chem. Toxicol.* **2014**, *65*, 185–195. [[CrossRef](#)] [[PubMed](#)]
46. Koh, P.O. Ferulic acid prevents the cerebral ischemic injury-induced decrease of Akt and Bad phosphorylation. *Neurosci. Lett.* **2012**, *507*, 156–160. [[CrossRef](#)]
47. Karthikeyan, S.; Kanimozhi, G.; Prasad, N.R.; Mahalakshmi, R. Radiosensitizing effect of ferulic acid on human cervical carcinoma cells in vitro. *Toxicol. In Vitro* **2011**, *25*, 1366–1375. [[CrossRef](#)]
48. Zueva, I.; Lushchekina, S.; Shulnikova, P.; Lenina, O.; Petrov, K.; Molochkina, E.; Masson, P. α -tocopherol, a slow-binding inhibitor of acetylcholinesterase. *Chem. Biol. Interact.* **2021**, *348*, 109646. [[CrossRef](#)]
49. Archer, C.R.; Hempenstall, S.; Royle, N.J.; Selman, C.; Willis, S.; Rapkin, J.; Blount, J.D.; Hunt, J. Testing the Effects of DL-Alpha-Tocopherol Supplementation on Oxidative Damage, Total Antioxidant Protection and the Sex-Specific Responses of Reproductive Effort and Lifespan to Dietary Manipulation in Australian Field Crickets (*Teleogryllus commodus*). *Antioxidants* **2015**, *4*, 768–792. [[CrossRef](#)]
50. Zhang, T.W.; Li, W.Z.; Xiao, H.N.; Jin, Y.C.; Wu, S.F. Recent progress in direct production of furfural from lignocellulosic residues and hemicellulose. *Bioresour. Technol.* **2022**, *354*, 127126. [[CrossRef](#)]
51. Nhien, L.C.; Long, N.V.D.; Lee, M. Novel hybrid reactive distillation with extraction and distillation processes for furfural production from an actual xylose solution. *Energies* **2021**, *14*, 1152. [[CrossRef](#)]
52. Zhang, X.; Xu, S.; Li, Q.; Zhou, G.; Xia, H. Recent advances in the conversion of furfural into bio-chemicals through chemo- and bio-catalysis. *RSC Adv.* **2021**, *11*, 27042–27058. [[CrossRef](#)]
53. Zawaneh, P.N.; Singh, S.P.; Padera, R.F.; Henderson, P.W.; Spector, J.A.; Putnam, D. Design of an injectable synthetic and biodegradable surgical biomaterial. *Proc. Natl. Acad. Sci. USA* **2010**, *107*, 11014–11019. [[CrossRef](#)]
54. de la Morena, S.; Acedos, M.G.; Santos, V.E.; Garcia-Ochoa, F. Dihydroxyacetone production from glycerol using *Gluconobacter oxydans*: Study of medium composition and operational conditions in shaken flasks. *Biotechnol. Progr.* **2019**, *35*, e2803. [[CrossRef](#)] [[PubMed](#)]
55. Albonetti, S.; Hu, C.W.; Saravanamurugan, S. Preface to Special Issue on Green Conversion of HMF. *ChemSusChem* **2022**, *15*, e202201057. [[CrossRef](#)]
56. Zhou, D.; Shen, D.; Lu, W.; Song, T.; Wang, M.; Feng, H.; Shentu, J.; Long, Y. Production of 5-Hydroxymethylfurfural from Chitin Biomass: A Review. *Molecules* **2020**, *25*, 541. [[CrossRef](#)]
57. Song, G.X.; Huang, D.X.; Li, H.J.; Wang, X.P.; Ren, Q.Q.; Jiang, L.; Wang, Y.; Su, S.; Hu, S.; Xiang, J. Pyrolysis reaction mechanism of typical Chinese agriculture and forest waste pellets at high heating rates based on the photo-thermal TGA. *Energy* **2022**, *244*, 123164. [[CrossRef](#)]
58. Kanca, A. Investigation on pyrolysis and combustion characteristics of low quality lignite, cotton waste, and their blends by TGA-FTIR. *Fuel* **2020**, *263*, 116517. [[CrossRef](#)]
59. Sait, H.H.; Hussain, A.; Salema, A.A.; Ani, F.N. Pyrolysis and combustion kinetics of date palm biomass using thermogravimetric analysis. *Bioresour. Technol.* **2012**, *118*, 382–389. [[CrossRef](#)]
60. nca-Couce, A.; Tsekos, C.; Retschitzegger, S.; Zimbardi, F.; Funke, A.; Banks, S.; Kraia, T.; Marques, P.; Scharler, R.; de Jong, W.; et al. Biomass pyrolysis TGA assessment with an international round robin. *Fuel* **2020**, *276*, 118002. [[CrossRef](#)]

61. Mishra, R.K.; Mohanty, K. Pyrolysis kinetics and thermal behavior of waste sawdust biomass using thermogravimetric analysis. *Bioresour. Technol.* **2018**, *251*, 63–74. [[CrossRef](#)]
62. Rami, J.M.; Patel, C.D.; Patel, C.M.; Patel, M.V. Thermogravimetric analysis (TGA) of some synthesized metal oxide nanoparticles. *Mater. Today* **2021**, *43*, 655–659. [[CrossRef](#)]
63. Hydrogenation of fast pyrolysis oil and model compounds in a two-phase aqueous organic system using homogeneous ruthenium catalysts. *J. Mol. Catal. A Chem.* **2007**, *264*, 227–236. [[CrossRef](#)]
64. Xing, J.K.; Kurose, R.; Luo, K.; Fan, J.R. Chemistry-Informed Neural Networks modelling of lignocellulosic biomass Pyrolysis. *Bioresour. Technol.* **2022**, *355*, 127275. [[CrossRef](#)] [[PubMed](#)]
65. Wang, B.; Xu, F.; Zong, P.; Zhang, J.; Tian, Y.; Qiao, Y. Effects of heating rate on fast pyrolysis behavior and product distribution of Jerusalem artichoke stalk by using TG-FTIR and Py-GC/MS. *Renew. Energ.* **2019**, *132*, 486–496. [[CrossRef](#)]
66. Elliott, D.C.; Hart, T.R. Catalytic Hydroprocessing of Chemical Models for Bio-oil. *Energ. Fuel.* **2017**, *23*, 631–637. [[CrossRef](#)]
67. Setiabudi, H.D.; Aziz, M.A.A.; Abdullah, S.; Teh, L.P.; Jusoh, R. Hydrogen production from catalytic steam reforming of biomass pyrolysis oil or bio-oil derivatives: A review. *Int. J. Hydrogen Energy* **2020**, *45*, 18376–18397. [[CrossRef](#)]
68. Atchimarungsri, T.; Gao, X.H.; Ma, Q.X.; Zhang, J.L.; Fan, S.B.; He, F.G.; Tian, J.M.; Reubroycharoen, P.; Zhao, T.S. Highly Efficient Conversion of Glycerol to Acetaldehyde Over In₂O₃/HZSM-5 Catalysts. *ACS Sustain. Chem. Eng.* **2022**, *10*, 11078–11087. [[CrossRef](#)]
69. Valentini, F.; Kozell, V.; Petrucci, C.; Marrocchi, A.; Gu, Y.L.; Gelman, D.; Vaccaro, L. Formic acid, a biomass-derived source of energy and hydrogen for biomass upgrading. *Energ. Environ. Sci.* **2019**, *12*, 2646–2664. [[CrossRef](#)]
70. Upadhyay, P.; Lali, A. Engineered *Pseudomonas putida* for biosynthesis of catechol from lignin-derived model compounds and biomass hydrolysate. *Prep. Biochem. Biotechn.* **2022**, *52*, 80–88. [[CrossRef](#)]
71. Yan, G.H.; Chen, G.F.; Peng, Z.Q.; Shen, Z.L.; Tang, X.; Sun, Y.; Zeng, X.H.; Lin, L. The Cross-Linking Mechanism and Applications of Catechol-Metal Polymer Materials. *Adv. Mater. Interfaces* **2021**, *8*, 2100239. [[CrossRef](#)]
72. Silvestre, F.; Aubry, J.M.; Benvegnu, T.; Brendle, J.; Durand, M.; Lavergne, A.; Len, C.; Molinier, V.; Mouloungui, Z.; Plusquellec, D.; et al. Agro-resources for a sustainable chemistry. *Actual. Chim.* **2010**, *338–339*, 28–40.
73. Liu, Y.; Wang, Y.G.; Dai, Y.J.; Bai, Y.Y.; Zhao, Q.X. Research on Combustion Properties and Pollutant Emission Characteristics of Blends of Maltol Byproduct/Pine Sawdust. *ACS Omega* **2022**, *7*, 325–333. [[CrossRef](#)] [[PubMed](#)]
74. Artigues, A.; Puy, N.; Bartroli, J.; Fabregas, E. Comparative Assessment of Internal Standards for Quantitative Analysis of Bio-oil Compounds by Gas Chromatography/Mass Spectrometry Using Statistical Criteria. *Energy Fuel.* **2014**, *28*, 3908–3915. [[CrossRef](#)]
75. Biswas, B.; Singh, R.; Kumar, J.; Singh, R.; Gupta, P.; Krishna, B.B.; Bhaskar, T. Pyrolysis behavior of rice straw under carbon dioxide for production of bio-oil. *Renew. Energ.* **2018**, *129*, 686–694. [[CrossRef](#)]
76. Ranaware, V.; Verma, D.; Insyani, R.; Riaz, A.; Kim, S.M.; Kim, J. Highly-efficient and magnetically-separable ZnO/Co@N-CNTs catalyst for hydrodeoxygenation of lignin and its derived species under mild conditions. *Green Chem.* **2019**, *21*, 1021–1042. [[CrossRef](#)]
77. Rambo, M.K.D.; Nemet, Y.K.S.; Junior, C.C.S.; Pedroza, M.M.; Rambo, M.C.D. Comparative study of the products from the pyrolysis of raw and hydrolyzed baru wastes. *Biomass Convers. Bior.* **2021**, *11*, 1943–1953. [[CrossRef](#)]
78. Hayashi, Y.; Komatsu, T.; Iwashita, K.; Fukusaki, E. H-1-NMR metabolomics-based classification of Japanese sake and comparative metabolome analysis by gas chromatography-mass spectrometry. *J. Biosci. Bioeng.* **2021**, *131*, 557–564. [[CrossRef](#)] [[PubMed](#)]
79. Kurihara, R.; Maruyama, I. Surface area development of Portland cement paste during hydration: Direct comparison with H-1 NMR relaxometry and water vapor/nitrogen sorption. *Cem. Concr. Res.* **2022**, *157*, 106805. [[CrossRef](#)]
80. Ostrowski, S.; Lopuszyliska, B.; Mikus, A. Shielding Effects in H-1 NMR Spectra of Halogen-Substituted meso-Tetraphenylporphyrin Derivatives. *Macroheterocycles* **2019**, *12*, 17–21. [[CrossRef](#)]
81. Xue, B.L.; Wen, J.L.; Sun, R.C. Lignin-Based Rigid Polyurethane Foam Reinforced with Pulp Fiber: Synthesis and Characterization. *ACS Sustain. Chem. Eng.* **2014**, *2*, 1474–1480. [[CrossRef](#)]
82. Wen, J.L.; Sun, S.L.; Yuan, T.Q.; Xu, F.; Sun, R.C. Understanding the chemical and structural transformations of lignin macromolecule during torrefaction. *Appl. Energ.* **2014**, *121*, 1–9. [[CrossRef](#)]
83. Kniat, A. Visualization of A Lifeboat Motion During Lowering Along Ship's Side. *Pol. Marit. Res.* **2017**, *24*, 42. [[CrossRef](#)]
84. Wani, S.A.; Najar, G.R.; Akhter, F. Characterization of available nutrients that influence pear productivity and quality in Jammu & Kashmir. *India J. Environ. Biol.* **2018**, *39*, 37.
85. Río, J.C.D.; Rencoret, J.; Marques, G.; Li, J.B.; Gellerstedt, G.; Jimenez-Barbero, J.; Martinez, A.T.; Gutierrez, A. Structural Characterization of the Lignin from Jute (*Corchorus capsularis*) Fibers. *J. Agr. Food Chem.* **2009**, *57*, 10271–10281.
86. Zhang, N.; Zhou, C.; Xia, W.; Nguyen, A.V. Volatilization of mercury in coal during conventional and microwave drying and its potential guidance for environmental protection. *J. Clean Prod.* **2018**, *176*, 1–6. [[CrossRef](#)]
87. Nongqwenga, N.; Modi, A.T. Phosphorus and potassium quantity/intensity properties of selected South African soils (Kwa-zulu-natal) and their correlation with selected soil parameters. *Appl. Ecol. Env. Res.* **2017**, *15*, 1–14. [[CrossRef](#)]
88. Wang, B.; Li, D.; Chen, T.; Qin, Z.; Peng, W.; Wen, J. Understanding the mechanism of self-bonding of bamboo binderless boards: Investigating the structural changes of lignin macromolecule during the molding pressing process. *BioResources* **2017**, *12*, 514–532. [[CrossRef](#)]
89. Wang, M.; Zhang, D.Q.; Su, J.; Dong, J.W.; Tan, S.K. Assessing hydrological effects and performance of low impact development practices based on future scenarios modeling. *J. Clean Prod.* **2018**, *179*, 12–23. [[CrossRef](#)]

90. Li, Y.Y.; Shaheen, S.M.; Rinklebe, J.; Ma, N.L.; Yang, Y.F.; Ashraf, M.A.; Chen, X.M.; Peng, W.X. Pyrolysis of *Aesculus chinensis* Bunge Seed with Fe₂O₃/NiO as nanocatalysts for the production of bio-oil material. *J. Hazard. Mater.* **2021**, *416*, 126012. [[CrossRef](#)]
91. Ge, S.B.; Shi, Y.; Xia, C.L.; Huang, Z.H.; Manzo, M.; Cai, L.P.; Ma, H.Z.; Zhang, S.; Jiang, J.C.; Sonne, C.; et al. Progress in pyrolysis conversion of waste into value-added liquid pyro-oil, with focus on heating source and machine learning analysis. *Energ. Convers. Manag.* **2021**, *245*, 114638. [[CrossRef](#)]
92. Li, Y.Y.; Li, G.Y.; Yang, Y.F.; Chen, X.M.; Peng, W.X.; Li, H.Y. Incorporation of Nanocatalysts for the Production of Bio-Oil from *Staphylea holocarpa* Wood. *Polymers* **2022**, *14*, 4385. [[CrossRef](#)]
93. Zhang, L.B.; Yang, X.; Sheng, Y.Q.; Huang, Q.G.; Yang, Z.L.; Shi, Y.; Guo, X.Q.; Ge, S.B. Influence of typical pretreatment on cotton stalk conversion activity and bio-oil property during low temperature (180–220) hydrothermal process. *Fuel* **2022**, *328*, 125250. [[CrossRef](#)]
94. Pu, Y.; Cao, S.; Ragauskas, A.J. Application of quantitative ³¹P NMR in biomass lignin and biofuel precursors characterization. *Energy Environ. Sci.* **2011**, *4*, 3154–3166. [[CrossRef](#)]

Disclaimer/Publisher’s Note: The statements, opinions and data contained in all publications are solely those of the individual author(s) and contributor(s) and not of MDPI and/or the editor(s). MDPI and/or the editor(s) disclaim responsibility for any injury to people or property resulting from any ideas, methods, instructions or products referred to in the content.